ORIGINAL PAPER

Imprinted Azorubine electrochemical sensor based upon composition of MnO$_2$ and 1-naphthylamine on graphite nanopowder

Somayyeh Piri[1] · Farideh Piri[1] · Mohammad Reza Yaftian[1] · Abbasali Zamani[2]

Abstract

A new sensitive and selective molecularly imprinted electrochemical sensor was developed for Azorubine determination. This sensor was based on molecularly imprinted polymer composed of poly(1-naphthylamine), triphenylamine (as cross-linkers) and dispersed MnO$_2$ nanorod particles on graphite nanopowders. The structure of the prepared nanocomposite was characterized by X-ray powder diffraction, energy-dispersive X-ray spectroscopy, field emission scanning electron microscopy, transmission electron microscopy and Fourier transform infrared spectroscopy. Calibration curve of the imprinted sensor was linear in the concentration range 1–12 mg L^{-1} with a detection limit of 0.57 mg L^{-1}. The application of the sensor was checked by the determination of Azorubine in a water sample.

Introduction

Natural and synthetic colors are extensively used in various food and cosmetic industries. Since natural food colors are relatively unstable and are more expensive than synthetic ones [1], a great amount of synthetic dyes are currently consumed in a variety of foods, drinks, candies, and sweets [2]. Although azo dyes are the largest group of dyes used in more than half of the global dye productions [3], some of them have been confirmed to be genetically toxic [4]. The permitted amount of these dyes is strictly regulated because of their potential risk to human health. The lists of permitted food colors vary from country to country [5]. Thus, monitoring and controlling the levels of dyes in food stuffs are of paramount importance [6, 7].

A great number of analytical techniques have frequently been used for the determination of food colorings [8–16]. These techniques include spectrophotometric methods [8, 9], thin-layer chromatography [10], voltammetry [11], polarography [12], capillary electrophoresis [13], ion chromatography [14], and high-performance liquid chromatography [15, 16]. However, some of these methods lack selectivity, need to complicated pretreatment and/or require relatively expensive apparatus.

The selective attitude of molecularly imprinted polymers (MIPs) allowed these materials to have recently been accepted widely as new prominent molecular recognition materials for preparing chemical sensors [17–22]. Their advantages such as stability, low cost and easy producibility relative to the similar biological species used in biosensors including antibodies and enzymes are among the highlighted characteristics of MIP-based sensors [20, 23, 24].

Various chemical sensors have been prepared using MIPs for molecular recognition followed by appropriate signal transductions such as impedimetric [25], potentiometric [26], voltammetry [27] and quartz crystal microbalance [28] techniques. Since electrochemical techniques allow sensitive, simple and inexpensive detection of a variety of analytes, it would be a promising alternative for dye analysis in food samples [12, 29–32].

Azorubine (disodium 4-hydroxy-3-(4-sulfonato-1-naphthylazo)-1-naphthalenesulfonate), named also Carmoisine, is an authorized food color, often used in European countries, but it is considered a violation in Norway, Sweden

✉ Mohammad Reza Yaftian
  yaftian@znu.ac.ir

[1] Department of Chemistry, Faculty of Science, University of Zanjan, Zanjan 45371-38791, Islamic Republic of Iran

[2] Department of Environmental Science, Faculty of Science, University of Zanjan, Zanjan 45371-38791, Islamic Republic of Iran

and the United States [33]. In the present work, the preparation of an Azorubine–MIP based on poly(1-naphthylamine) (PNA) and manganese oxide (MnO_2) nanocomposite on graphite nanopowders (Gr), abbreviated as PNA@MnO_2/Gr, is reported. The synthesis and characterization of the Azorubine–molecularly imprinted PNA@MnO_2/Gr nanocomposite are reported in detail. MnO_2 was used because it is suggested that it increases the nanocomposite conductivity. Furthermore, the interaction of MnO_2 with both Azorubine and aniline monomers during polymerization leads to a more efficient imprinting process, and the presence of MnO_2 allows also a better adhesion of the graphene oxide and polymer. The prepared MIP was used for the preparation of Azorubine-selective voltammetric sensor. The applicability of the sensor was examined by determination of Azorubine in water samples.

Experimental

Materials and methods

1-Naphthylamine (for synthesis, Merck), triphenylamine (for synthesis, Merck), Azorubine (analytical standard, Sigma-Aldrich), ethanol (Ph Eur, Merck), hydrochloric acid (puriss, Fluka), sulfuric acid (GR for analysis, Merck), nitric acid (suprapur, Merck), sodium hydroxide (pellets, Merck), ammonium persulfate (reagent grade, Sigma-Aldrich), potassium chloride (extra pure, Merck), potassium permanganate (for analysis, Merck) and graphite (Merck Millipore) were used for the synthesis of the studied MIP and preparation of the Azorubine electrochemical sensor. Deionized water (resistance ≥ 18.2 MΩ cm) was used throughout the experiments and was provided by a water purification system (Zolalan, M-UV-3$^+$, Iran). Electrochemical measurements were performed on a three-electrode system voltammeter (Metrohm 797 VA Computrace, Switzerland). The working electrode was composed of a layer of the molecularly imprinted nanocomposite PNA@MnO_2/Gr connected to the voltammeter by a copper wire. The auxiliary and reference electrodes were a platinum wire and a saturated calomel electrode, respectively. Nanophase materials were characterized by field emission scanning electron microscopy (FE-SEM, Mira 3-XMU system, USA). The X-ray powder diffraction patterns were recorded on a Brucker XRD diffractometer (B8-Advance, Germany) using Cu Kα radiation in the range $2\theta = 5$–$60°$ at 40 kV. Fourier transform infrared spectra were obtained using a FT-IR Bruker Vector 22 (Germany) spectrophotometer. Transmission electron microscopy (TEM) observations were carried out using a Philips instrument (model CM120, Holland) with an image analysis system apparatus. An ultrasonic cleaner Codyson (model CD-4820, China) bath which worked at 170 W power and

50/60 Hz was used for ultrasonic irradiations. Centrifugations were assisted with a centrifuge Heraeus (Labofuge 300, Germany).

Preparation of MnO_2/Gr and molecularly imprinted PNA@MnO_2/Gr synthesis

A mixture of graphite (0.40 g) and potassium permanganate (10.54 g) in 100 mL of sulfuric acid (2 mol L^{-1}) was stirred for 72 h at 100 °C. This mixture was then dispersed with sonication for 30 min. The product was separated by centrifugation, washed with deionized water and dried at room temperature. In this procedure, MnO_2/graphite (MnO_2/Gr) was obtained by low oxidation of graphite surface and reduction of permanganate ion to manganese dioxide. Then, a mixture of 1-naphthylamine (0.25 g), nanocomposite MnO_2/Gr (0.10 g), 0.21 g of the cross-linker triphenylamine and 0.20 g Azorubine in 60 mL of mixed ethanol/water (3:1 V/V) solvent was sonicated for 30 min. Polymerization took place by the addition of ammonium persulfate (0.20 g) to the mixture under ultrasonic irradiation for a further 80 min at 30–50 °C. The product (PNA@MnO_2/Gr) was washed thoroughly with mixed ethanol/water (5:3 V/V) solvent. Non-imprinted (NIP) nanocomposite PNA@MnO_2/Gr was synthesized in the same way except that the template molecule (Azorubine) was absent. The route of the preparation of MnO_2/Gr and the synthesis of the studied MIP are illustrated in Fig. 1.

Preparation of the Azorubine sensor

To prepare the working electrode for Azorubine, the synthesized PNA@MnO_2/Gr-imprinted nanocomposite powder was added to the silicon oil mixed with a stainless steel spatula, the excess of silicon oil was taken off with the aid of a sheet of paper. The final paste was used to fill a hole (3 mm in diameter, 1 mm in depth) at the end of an electrode body. This layer was connected to the voltammeter by a copper wire. The sensor performance was evaluated by cyclic voltammetric system using the prepared sensor in hydrochloric acid solution (0.1 mol L^{-1}) in the applied voltage range −1 to 0.3 V.

Results and discussion

Preparation of the Azorubine–MIP

Graphite nanopowder anchored with nanoparticle manganese oxide was prepared by an in situ one-pot procedure. During the reaction, the reduction of potassium permanganate to manganese dioxide nanorod, and the oxidation of graphite surface occur simultaneously. This allowed the

Fig. 1 Schematic representation of the anchoring of MnO$_2$ nanoparticles on graphite nanopowders (**a**) and the synthesis of Azorubine–imprinted nanocomposite PNA@MnO$_2$/Gr (**b**)
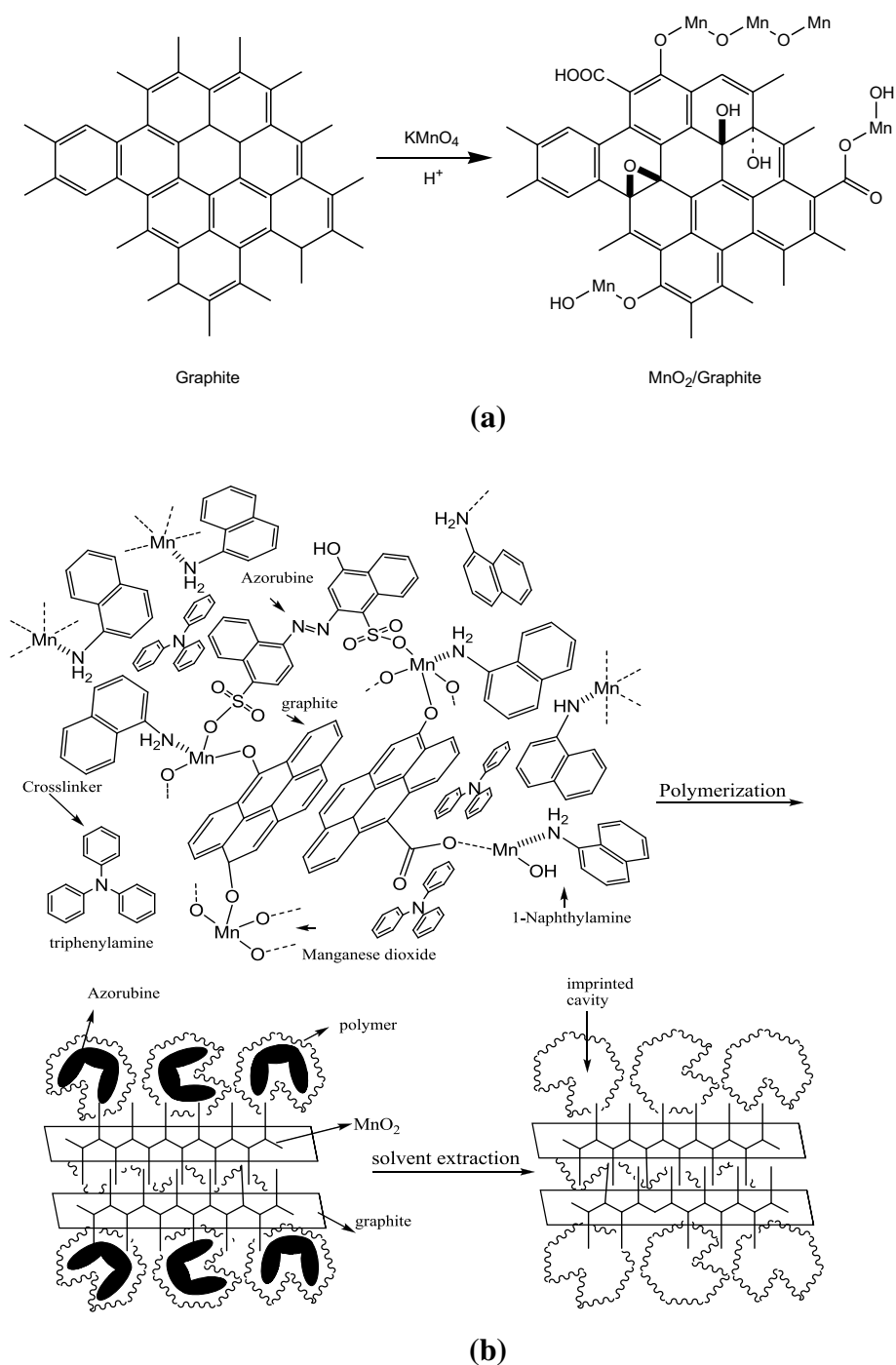
formation of MnO$_2$/Gr nanocomposite structure, including nanorods of MnO$_2$. The space between these nanoparticles was filled by nanopowder graphite (Fig. 1). It is noteworthy that the presence of graphite improves significantly the conductance of MnO$_2$ nanorods.

The synthesis of molecularly imprinted nanocomposite of PNA@MnO$_2$/Gr and their corresponding non-imprinted nanocomposite (NIP) was carried out using a bulk polymerization method. The MIP and the corresponding NIP were prepared using 1-naphthylamine as the monomer. The amine functionalities in this monomer allowed the interaction with the template (i.e. Azorubine molecule), leading to the formation of well-defined imprinted cavities. The template was then removed from Azorubine–MIP materials by the extraction of Azorubine using a mixture of ethanol/water (1:1 V/V), to afford the free imprinted cavities for the selective rebinding of the template molecules.

Characterization

The FT-IR spectra of PNA and PNA@MnO$_2$/Gr are shown in Fig. 2. The spectra of PNA (Fig. 2a) showed the wavenumber bands at 3355 and 2924 cm^{-1} corresponding to N–H stretching of amine and aromatic C–H stretching in PNA skeleton, respectively. The absorption peaks corresponding to imine stretching mode appear at 1732 and 1653 cm^{-1}, while the peak at 1594 cm^{-1} is assigned to the N=Q=N quinonoid ring skeletal (Q) vibrations, and the peak at 1506 cm^{-1} appears due to N–B–N, benzenoid ring skeletal (B) vibrations. The band located at 1290 cm^{-1} is attributed to the C–N stretching vibration of an aromatic amine. The peak at 1156 cm^{-1} corresponds to BNH$^+$=Q and B–NH–B vibrations [34]. The presence of peaks at 769 cm^{-1} is consistent with the polymerization of 1-naphthylamine through N–C linkages. A comparison of the spectrum of PNA with that of PNA@MnO$_2$/Gr (Fig. 2b) allowed attributing the
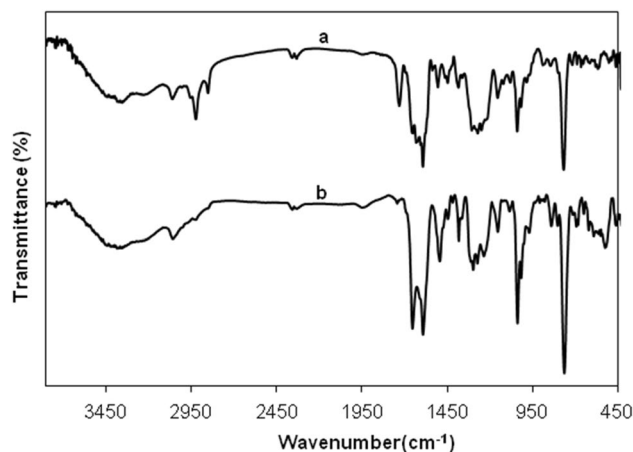
band at 524 cm^{-1} of the latter to the Mn–O vibration. The other significant peaks in the FT–IR spectrum of the nanocomposite PNA@MnO$_2$/Gr were almost the same described in the PNA spectrum. The interaction of MnO$_2$ and PNA made the peaks of PNA shift slightly to the lower wavenumbers in peak position and obviously weaken peak intensities with respect to that of PNA.

Figure 3 includes the FE-SEM images of the MnO$_2$ nanorods (a), the distribution of the MnO$_2$ nanoparticles (b), and the SEM images of the Azorubine–molecularly imprinted polymer (c). These images confirmed a size of ~20 nm for the formed manganese dioxide rods and their homogeneous dispersion on the surface of graphite nanopowders.

The chemical composition of the prepared PNA@MnO$_2$/Gr nanocomposite was examined by EDX spectrum (Fig. 4). This spectrum depicts the presence of C, N, O, Mn and Au elements in the sample. The presence of carbon, nitrogen and oxygen can be attributed to the organic components of PNA and graphene. The presence of signals of manganese signifies the anchored manganese dioxide in the structure of the prepared nanocomposite. The signal of gold resulted from the cover used for EDX analysis. The corresponding peaks of carbon, nitrogen, oxygen and manganese elements approved the PNA@MnO$_2$/Gr nanocomposite formation.

The prepared TEM of the nanocomposite PNA@MnO$_2$/Gr showed that MnO$_2$/Gr powder is totally covered by the polymer (Fig. 4). The XRD pattern of PNA@MnO$_2$/Gr (Fig. 4) contains seven characteristic peaks at 2θ values of 8.9°, 18.1°, 25.8°, 28.8°, 37.6°, 46.0°, 49.8° which was consistent with the standard XRD data for MnO$_2$ (JCPDS card no. 00-044-0141) and the peaks at 7.9°, 15.9°, 23.9°, 32.1°, 40.4°, 46.6°, 52.2°, 57.9° (JCPDS card no. 01-074-2328) for graphite nanopowder. These characteristics approved the attachment of MnO$_2$ nanoparticles on the surface of the graphite nanopowder.
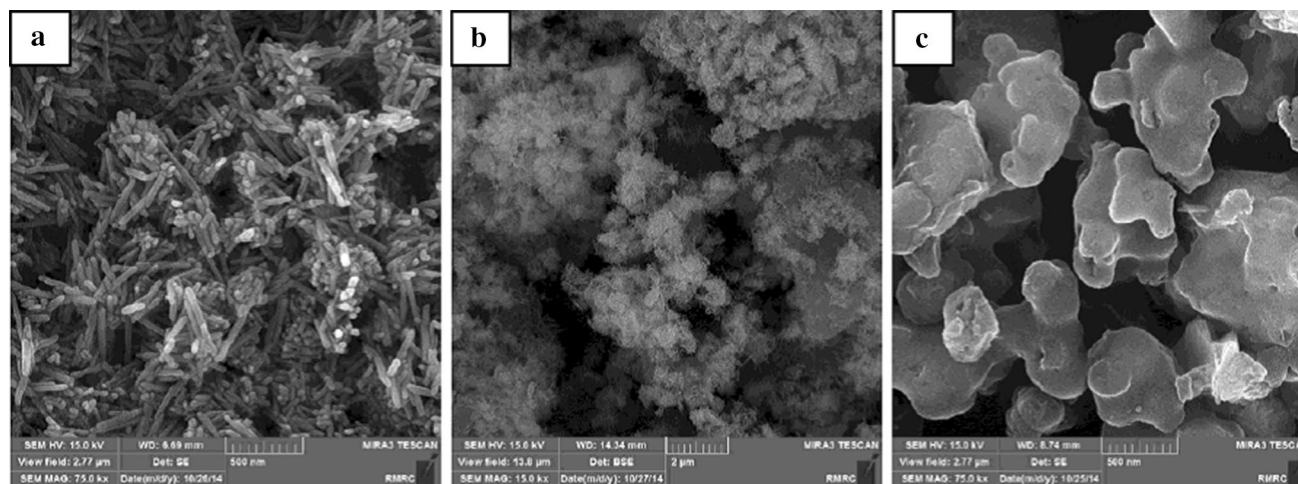

Fig. 2 FT-IR spectra of PNA (**a**) and PNA@MnO$_2$/Gr (**b**)

Fig. 3 FE-SEM images of **a** MnO$_2$ nanorod, **b** MnO$_2$/Gr nanocomposite and **c** PNA@MnO$_2$/Gr nanocomposites
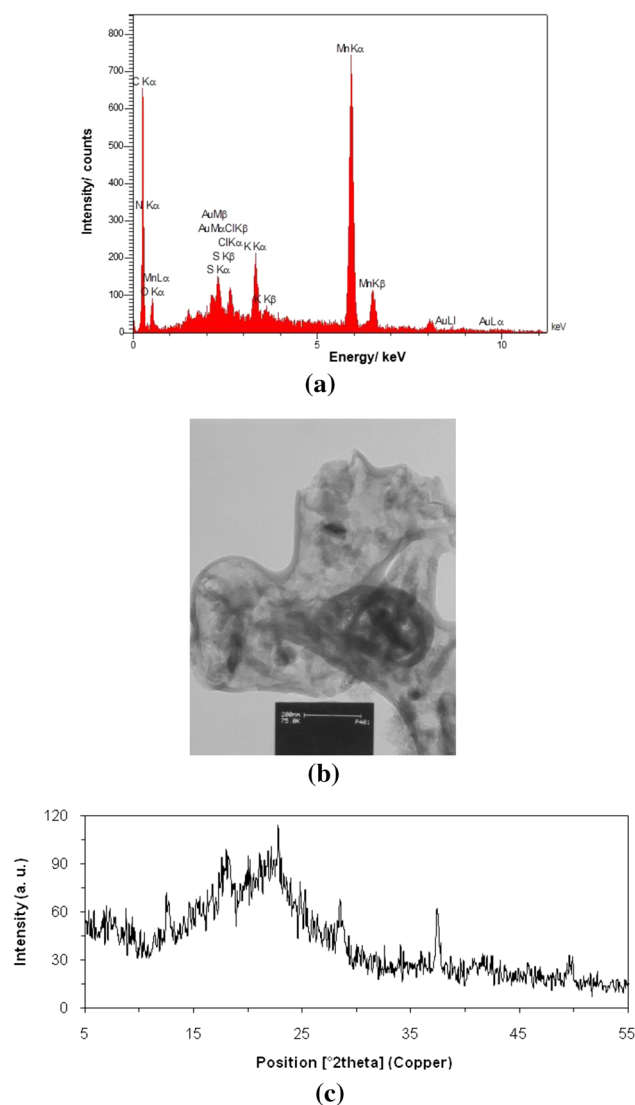
(a)

(b)

(c)

Fig. 4 The EDX spectrum of PNA@MnO$_2$/Gr nanocomposite, TEM and the XRD pattern of non-imprinted PNA@MnO$_2$/Gr

Azorubine–MIP sensor

The cyclic voltammetry (CV) as a sensitive electrochemical method was used for examining the ability of the prepared Azorubine–MIP sensor designed for the determination of Azorubine. The prepared sensors based on the PNA@MnO$_2$/Gr nanocomposite immersed in a solution of hydrochloric acid (0.1 mol L^{-1}) were used as indicator electrodes for verifying its electrochemical behavior in cyclic voltammetry experiments. The potential applied onto the electrodes was swept in the range −1 to +0.3 V, at a scan rate of 0.1 V s^{-1}. The cyclic voltammograms of the copper wire electrode modified with the Azorubine–MIP and that of non-imprinted (NIP)
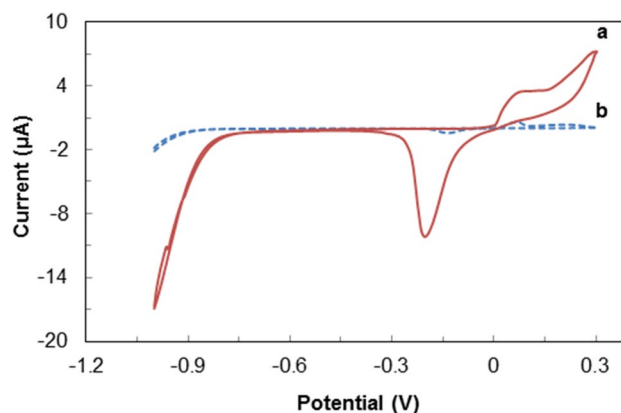

Fig. 5 Cyclic voltammograms of Azorubine obtained using the indicator electrodes based on the Azorubine–MIP (**a**) and that of the NIP (**b**) nanocomposite PNA@MnO$_2$/Gr. Experimental conditions: concentration of Azorubine 6 mg L^{-1} in hydrochloric acid (0.1 mol L^{-1}); scan rate 0.1 V s^{-1}

PNA@MnO$_2$/Gr nanocomposite in hydrochloric acid solution (0.1 mol L^{-1}) containing Azorubine (6 mg L^{-1}) are depicted in Fig. 5.

The obtained cyclic voltammograms (CV) on the MIP electrode showed a significant reduction peak at −0.2 V and oxidation peak at 0.06 V, at the scan rate of 0.1 V s^{-1}. The CV of the electrode covered with NIP presented a small peak at about 0.06 V. This indicated the nonspecific adsorption of Azorubine on the MIP and the pronounced role of the MIP on the response of the sensor to Azorubine.

Anodic and cathodic peaks that appeared in the forward and reverse scans, respectively, suggested a quasi-reversible electrochemical attitude of Azorubine at the surface of the indicator electrode. The presence of cathodic peak current observed for PNA@MnO$_2$/Gr was described by considering the reduction of the azo group to amine in a single-step process. These data are also important to assess the feasibility of the electrochemical degradation of azo dyes [35]. A suggestion for the mechanism of the azo group reduction process in acidic media can be expected as a two-step process shown below:
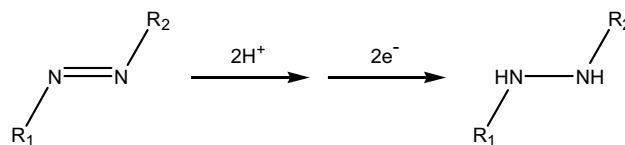
It is noteworthy that for such reduction process, in neutral or weak acid media, some two or three electron reduction mechanisms resulting in hydrazo compounds as final products have been proposed [36].
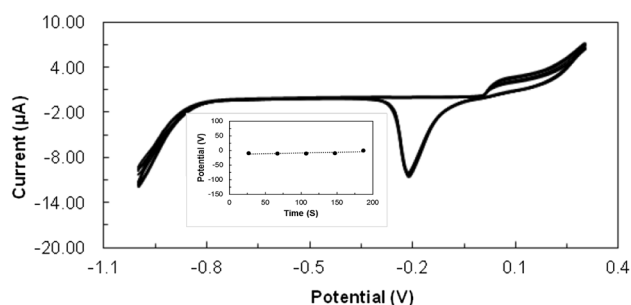
Fig. 6 Recorded cyclic voltammograms of a solution of Azorubine 6 mg L^{-1} in hydrochloric acid (0.1 mol L^{-1}); scan rate 0.1 V s^{-1}, at different time between 25 and 180 s
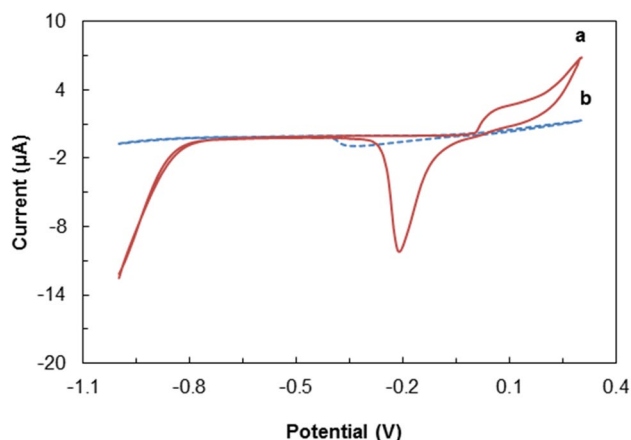

Fig. 7 Cyclic voltammograms of Azorubine (**a**) and Rhodamine B (**b**) using the electrode prepared based on the Azorubine–imprinted polymer PNA@MnO$_2$/Gr. Experimental conditions: concentration of Azorubine and Rhodamine B 6 mg L^{-1}; electrolyte 0.1 mol L^{-1} HCl; scan rate 0.1 V s^{-1}

Fig. 8 CV diagrams of the reduction currents of various concentrations of Azorubine in 0.1 mol L^{-1} of hydrochloric acid and scan rate 0.1 V s^{-1}

Fig. 9 Calibration curve of the investigated MIP-modified sensor's response as a function of Azorubine concentration. Error bars are ±standard deviation for $1\sigma_{n-1}$ ($n = 3$)

The cyclic voltammograms and the potentials correspond to the current peaks of the electrodes contacting with Azorubine solutions (1, 3, 6 and 12 mg L^{-1}) in the range 25–180 s before recording the cyclic voltammograms. As instance, the cyclic voltammograms and the potentials of the current peaks for the solution of 6 mg L^{-1} are shown in Fig. 6. An independency to the contact time, in the studied range, of the electrode response confirmed the reversibility and rapid binding of the analyte by the investigated MIP.

Characteristics of the prepared sensor

To evaluate the selective behavior of the prepared sensor toward Azorubine, its cyclic voltammogram (6 mg L^{-1}) in a 0.1 mol L^{-1} of hydrochloric acid and with a scan rate of 0.1 V s^{-1} was compared with that of Rhodamine B under the same conditions. This dye was tested because the unauthorized use of this dye in food products in place of Azorubine
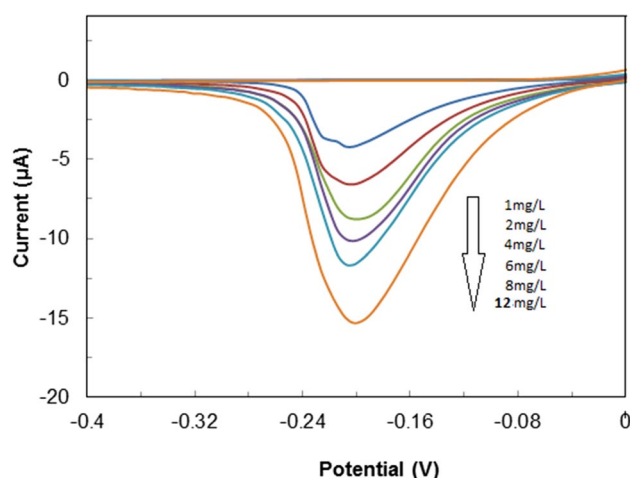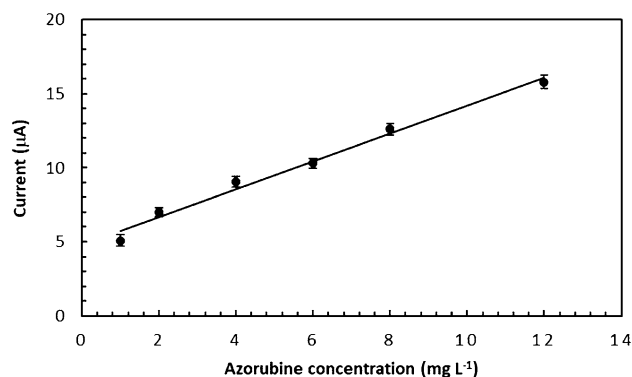
is illegal sometimes. The results are shown in Fig. 7. This comparison showed the excellent selectivity of the prepared sensor based on the imprinted PNA@MnO$_2$/Gr nanocomposite toward Azorubine.

The examination of the voltammetric response of the investigated sensor as a function of the Azorubine concentration (Fig. 8) has proved the linear response of the electrode in the range 1–12 mg L^{-1} of Azorubine, in 0.1 mol L^{-1} solution of hydrochloric acid. The corresponding calibration curve is shown in Fig. 9. The linear equation at potential -0.2 V was $i = 0.94\,C_{Azorubine} + 4.80$ (with $R^2 = 0.98$), in which "i" is the absolute current in µA, and $C_{Azorubine}$ is the Azorubine concentration in mg L^{-1}. Linear calibration model was used to compute the LOD and LOQ using the equations $LOD = 3s_{blk}/m$ and $LOQ = 10s_{blk}/m$, where s_{blk} is the standard deviation of the blank response and m is the

Table 1 Comparison of different electrochemical methods in the determination of Azorubine

Electrode	Method	LDR[a] (mg L^{-1})	LOD[b] (mg L^{-1})	LOQ[c] (mg L^{-1})	Investigated interference	References
Mercury	DPP	0.02-4.0	–[d]	0.042	Ponceau 4R, Allura red	[37]
Bismuth film/glassy carbon	DPV	0–60	3	9	Amaranth, Poceau, Allura red	[38]
MWCNT/glassy carbon	DPV	0.27–2.5	0.06	–[d]	Tetrazine, sunset yellow	[39]
NiO/CNTs/carbon paste	CV	35–327	0.01	–[d]	Tetrazine	[40]
MnO$_2$/1-naphthylamine/graphite	CV	1–12	0.57	1.92	Rhodamine B 6	This work

[a]Linear dynamic range

[b]Limit of detection

[c]Limit of quantification

[d]Not reported

slope of the calibration curve. The estimated LOD and LOQ were 0.57 and 1.92 mg L^{-1}, respectively.

Characteristics and analytical performances of the developed sensor together with those of some previously reported electrochemical sensors for the determination of Azorubine are shown in Table 1.

Application of the sensor

The application of the proposed MIP electrochemical sensor was evaluated by the determination of spiked Azorubine in a well water sample (University of Zanjan campus, Zanjan, Iran). 50 mL portions of the sample, acidified to 0.1 mol L^{-1} with HCl, were spiked with different amounts of Azorubine. The final concentration of the analyte in these samples ranged 1–12 mg L^{-1}. Each solution was used for three independent cyclic voltammetric determinations. The variation in determined currents, at potential -0.2 V, as a function of Azorubine concentration gives a straight line ($i = 0.89 \, C_{Azorubine} + 3.97$; $R^2 = 0.97$), showed the ability of the prepared sensor for the determination of Azorubine in such samples.

Conclusions

MnO$_2$ nanorod particles were in situ grown on the nanopowder of graphite. The PNA@MnO$_2$/Gr nanocomposite was prepared via polymerization of 1-naphthylamine on the surface of MnO$_2$/Gr nanocomposite. Azorubine molecularly imprinted PNA@MnO$_2$/Gr nanocomposite was successfully applied for the preparation of an Azorubine sensor. The proposed sensor offered the simplicity in design and short measuring time. It exhibited a wide linear calibration range, a good sensitivity and repeatability. This sensor was applied for the determination of Azorubine in a well water sample with satisfactory results.

References

1. A. Giuliani, L. Cerretani, A. Cichelli, Colors: Properties and Determination of Natural Pigments A2—Caballero, Benjamin, in *Encyclopedia of Food and Health*, ed. by P.M. Finglas, F. Toldrá (Academic Press, Oxford, 2016), p. 273
2. W.E. Diacu, Colors: Properties and Determination of Natural Pigments A2—Caballero, Benjamin, in *Encyclopedia of Food and Health*, ed. by P.M. Finglas, F. Toldrá (Academic Press, Oxford, 2016), p. 284
3. K. Yamjala, M.S. Nainar, N.R. Ramisetti, Food Chem. **192**, 813 (2016)
4. F.M.D. Chequer, T.M. Lizier, R. de Felício, M.V.B. Zanoni, H.M. Debonsi, N.P. Lopes, D.P. de Oliveira, Toxicol. In Vitro **29**, 1906 (2015)
5. P. Amchova, H. Kotolova, J. Ruda-Kucerova, Regul. Toxicol. Pharm. **73**, 914 (2015)
6. V. Peksa, M. Jahn, L. Štolcová, V. Schulz, J. Proska, M. Procházka, K. Weber, D. Cialla-May, J.R. Popp, Anal. Chem. **87**, 2840 (2015)
7. M. Pávai, T. Szabó, A. Paszternák, Cellulose **22**, 1883 (2015)
8. M.J. Scotter, *Colour Additives for Foods and Beverages* (Woodhead Publishing, Oxford, 2016), p. 131
9. R. Gürkan, N. Altunay, J. Food Compos. Anal. **42**, 141 (2015)
10. F. Gao, Y. Hu, D. Chen, E.C. Li-Chan, E. Grant, X. Lu, Talanta **3**, 344 (2015)
11. A. Masek, E. Chrzescijanska, M. Zaborski, Food Chem. **148**, 18 (2014)
12. U.T. Yilmaz, F. Ergun, H. Yilmaz, J. Food Drug Anal. **22**, 329 (2014)
13. A.M. López-Montes, A.-L. Dupont, B. Desmazières, B. Lavédrine, Talanta **114**, 217 (2013)
14. F.I. de Andrade, M.I.F. Guedes, ÍG.P. Vieira, F.N.P. Mendes, P.A.S. Rodrigues, C.S.C. Maia, M.M.M. Ávila, L. de Matos Ribeiro, Food Chem., **157**, 193 (2014)
15. J.H. Lee, M.-G. Choung, Food Chem. **124**, 1217 (2011)
16. P. Qi, Z. Lin, G. Chen, J. Xiao, J. Zhou, Z.-A. Liang, L.-N. Luo, X.-W. Zhang, Food Chem. **181**, 101 (2015)
17. Y.-B. Wei, Q. Tang, C.-B. Gong, M.H.-W. Lam, Anal. Chim. Acta **900**, 10 (2015)

18. M.V. Foguel, X.-A. Ton, M.V. Zanoni, T.S. Maria, K. Del Pilar, B.T.S. Haupt, Bui, Sens. Actuators B **218**, 222 (2015)
19. K. Kor, K. Zarei, Talanta **146**, 181 (2016)
20. G. Yang, F. Zhao, Sens. Actuators B **220**, 1017 (2015)
21. M. Bougrini, A. Florea, C. Cristea, R. Sandulescu, F. Vocanson, A. Errachid, B. Bouchikhi, N. El Bari, N. Jaffrezic-Renault, Food Control, **59**, 424 (2016)
22. H.-H. Li, H.-H. Wang, W.-T. Li, X.-X. Fang, X.-C. Guo, W.-H. Zhou, X. Cao, D.-X. Kou, Z.-J. Zhou, S.-X. Wu, Sens. Actuators B **222**, 1127 (2016)
23. Q. Wang, M. Chen, H. Zhang, W. Wen, X. Zhang, S. Wang, Sens. Actuators B **222**, 264 (2016)
24. H. Niu, Y. Yang, H. Zhang, Biosens. Bioelectron. **74**, 440 (2015)
25. V. Ratautaite, S.D. Janssens, K. Haenen, M. Nesládek, A. Ramanaviciene, I. Baleviciute, A. Ramanavicius, Electrochim. Acta **130**, 361 (2014)
26. T.S. Anirudhan, S. Alexander, Biosens. Bioelectron. **64**, 586 (2015)
27. S. Sadeghi, A. Motaharian, Mat. Sci. Eng. C **33**, 4884 (2013)
28. M.R. Eslami, N. Alizadeh, Sens. Actuators B **220**, 880 (2015)
29. B. Claux, O. Vittori, Electroanalysis **19**, 2243 (2007)
30. A. Królicka, A. Bobrowski, J. Zarębski, I. Tesarowicz, Electroanalysis **26**, 756 (2014)
31. T. Gan, J. Sun, W. Meng, L. Song, Y. Zhang, Food Chem. **141**, 3731 (2013)
32. S. Chandran, L.A. Lonappan, D. Thomas, T. Jos, K.G. Kumar, Food Anal. Methods **7**, 741 (2014)
33. A. Thiam, I. Sirés, E. Brillas, Water Res. **81**, 178 (2015)
34. U. Riaz, S. Ahmad, S.M. Ashraf, Nanoscale Res. Lett. **3**, 45 (2008)
35. M. Arvin, G. Dehghan, M.A. Hosseinpourfeizi, A.A. Moosavi-Movahedi, Spectrosc. Lett. **46**, 250 (2013)
36. A.H. Gemeay, Dyes Pigments **54**, 201 (2002)
37. S. Chanlon, L. Joly-Pottuz, M. Chatelut, O. Vittori, J.L. Cretier, J. Food. Compost. Anal. **18**, 503 (2005)
38. B. Claux, O. Vittori, Electroanalysis **19**, 2243 (2007)
39. P. Sierra-Rosales, C. Toledo-Neira, J.A. Squella, Sens. Actuators B **240**, 1257 (2017)
40. M. Bijad, H. Karimi–Maleh, M. Farsi, S.A. Shahidi, J. Food Meas. Charact. **12**, 634 (2018)